

Viewpoint Paper

# Wetting in high-temperature materials processing: The case of Ni/MgO and NiW10/MgO

N. Sobczak,<sup>a,\*</sup> R. Nowak,<sup>a</sup> R. Asthana<sup>b</sup> and R. Purgert<sup>c</sup>

<sup>a</sup>Foundry Research Institute, Zakopianska St. 73, 30418 Cracow, Poland

<sup>b</sup>Department of Engineering & Technology, University of Wisconsin-Stout, Menomonie, WI 54751, USA

<sup>c</sup>Energy Industries of Ohio, Park Center Plaza, Suite 200, 6100 Oak Tree Boulevard, Independence, OH 44131, USA

Received 25 January 2010; revised 25 February 2010; accepted 1 March 2010

Available online 6 March 2010

**Abstract**—The wetting behavior of liquid Ni and NiW10 on MgO(1 0 0) single crystals was examined by the sessile drop method at 1773 K in flowing Ar. A special procedure was used for in situ opening of the Ni/MgO and NiW10/MgO interfaces directly during wettability test at high temperature. Scanning probe microscopy revealed evidence of strong surface modification of MgO(1 0 0) during wettability tests that was found to be affected by metal evaporation, the chemistry of the liquid metal and the primary oxide film. © 2010 Acta Materialia Inc. Published by Elsevier Ltd. All rights reserved.

**Keywords:** Triple line; Sessile drop; Ridging; Scanning probe microscopy

## 1. Introduction

Metal–ceramic interfaces play a key role in many modern materials, and scientific knowledge about metal–ceramic interactions is of central importance to designing and developing materials. Metal–ceramic interactions structure and are structured by complex surface and interface processes across length scales. Such processes include but are not limited to grain boundary grooving [1], ridging and dissolution at the triple line (TL) [2,3], atomic transport at the TL [4–7], adsorption and local reactions [8,9], ceramic faceting, coarsening and roughening [10–15].

Because of experimental difficulties, direct observations of metal–ceramic interactions and interface evolution at high temperatures are prohibitively difficult (although there have been notable attempts at in situ atomic-scale observations of reactive wetting fronts [16]). In general, metal–ceramic interactions are examined after removal of the metal droplet to make the modified ceramic surface amenable to examination (e.g. [5]). This, however, precludes the possibility of investigating the topology of ceramic substrates or wetting front morphology directly during high-temperature testing or processing.

It is well known that for polycrystalline ceramics, grain boundary grooving [1] results in significant roughening of the ceramic substrate, thus strongly affecting the contact angle,  $\theta$ , formed on such surfaces [17]. Surface roughening via faceting can also occur even in single-crystal substrates subjected to high-temperature annealing (e.g. MgO [18–21] or Al<sub>2</sub>O<sub>3</sub> [22] single crystals); it was found to be responsible for an unusual increase in  $\theta$  with time at  $T < 1200$  °C in Al/ $\alpha$ -Al<sub>2</sub>O<sub>3</sub>(0 0 0 1) [22] despite the fact that the surface structural transformation during wettability tests was never confirmed experimentally due to its reversibility, as suggested in Ref. [22]. In the context of wettability studies, therefore, it would be useful to examine, if feasible, the substrate structure as it is modified during drop spreading. This could be accomplished using the experimental system developed at the Foundry Research Institute [23] that permits multiple functions including drop pushing, smearing and rubbing.

The Ni/MgO and NiW10/MgO systems were used for the study because of their importance in modern science and technology. MgO is utilized in many advanced ceramics used for measurements of the thermophysical properties of materials or for melting technology products (molds, filters, crucibles, etc.). Since MgO-rich inclusions are the most common defects in Ni-superalloy castings, understanding their formation presents an important technological issue. MgO is also useful as a substrate for epitaxial growth of thin films or as Ni/MgO catalyst. Various MgO nanostructures can be

\* Corresponding author. Tel.: +48 12 2618526; fax: +48 12 2660870; e-mail addresses: [natalie@iod.krakow.pl](mailto:natalie@iod.krakow.pl); [nataliesobczak@interia.pl](mailto:nataliesobczak@interia.pl)

obtained through diverse synthesis routes [24] and, for their further utilization, research at the nanoscale is needed. Additionally, Ni/MgO and NiW10/MgO are good as model systems for characterizing the interfaces at the nanoscale as high-quality, high-purity and optically clear MgO single crystals are commercially available in large sizes and neither chemical reaction nor significant metal evaporation in Ar takes place in these systems.

## 2. Experimental procedure

The materials used were high-purity (>99.95%) single-crystalline MgO ( $\text{MgO}^{\text{SC}}$ ), pure Ni (99.99%) and NiW10 alloy (10 wt.% W) made by arc melting high-purity (99.99%) Ni and W. The  $\text{MgO}^{\text{SC}}$  substrates of size  $10 \text{ mm} \times 10 \text{ mm} \times 1 \text{ mm}$  and of  $(1\ 0\ 0) \pm 0.2^\circ$  crystallographic orientation were prepared from MgO (cubic,  $a = 4.216 \text{ \AA}$ ) crystals (maximum size:  $50.8 \text{ mm} \times 50.8 \text{ mm} \times 2.54 \text{ mm}$ ; density  $3.58 \text{ kg m}^{-3}$ ; coefficient of thermal expansion (CTE)  $= 12.8 \times 10^{-6} \text{ K}^{-1}$ ) by MIT Corp. (USA) using arc melting coupled with EPI polishing of as-cleaved substrates to a roughness of  $R_a < 10 \text{ \AA}$  before packing the samples into a sealed container for transportation. The crystals were free of inclusions and micro-cracks and contained (in ppm)  $\text{Ca} \leq 40$ ,  $\text{Al} \leq 15$ ,  $\text{Si} \leq 10$ ,  $\text{Fe} \leq 50$ ,  $\text{Cr} \leq 10$ ,  $\text{B} \leq 5$  and  $\text{C} \leq 10$ .

The wettability of  $\text{MgO}(1\ 0\ 0)$  substrates was studied at 1773 K for 15 min under high-purity flowing Ar by the sessile drop technique and contact heating ( $10 \text{ K min}^{-1}$ ), using the experimental system described in Ref. [23]. Prior to placing the metal samples into the vacuum chamber, their surfaces were cleaned mechanically and ultrasonically in acetone and isopropanol for 5 min each. Immediately after opening the sealed container, the  $\text{MgO}^{\text{SC}}$  substrate was placed together with the metal sample in the small load-lock (pre-treatment) chamber of the experimental unit where a vacuum of  $10^{-6} \text{ mbar}$  was produced by a membrane and turbomolecular pump in 0.5 h and the couple was preheated (423 K, 15 min) to remove adsorbed gases. Then it was transferred through the intermediate ultra-

high vacuum (UHV) chamber ( $10^{-7} \text{ mbar}$ , ionic pump) to the UHV chamber ( $10^{-7} \text{ mbar}$ , turbomolecular pump) for the wettability test. These chambers do not contact air and all pumps work continuously.

The test unit [23] permits suction of a drop via an overhead alumina capillary for in situ drop removal and opening of the drop–substrate interface at high temperatures directly in the UHV chamber. However, for certain couples, this procedure could not be applied because the lightweight MgO substrate strongly adhered to the drop, and was picked up along with the drop, thus preventing drop–substrate separation, similar to that reported for Ni/ $\text{Al}_2\text{O}_3^{\text{SC}}$  in Ref. [25]. Therefore, an alternative procedure employing two manipulators was used for simultaneous movement of the upper alumina capillary and sideways “pushing” of the drop with an alumina support to either replace the drop in a new position (with Ni drop) or slide it onto another substrate (with NiW10 drop). Even sideways drop pushing led to problems with separation because the strong adhesion caused the drop to move together with the substrate. Therefore, a specially designed support with a fixture was made of a perfectly flat and horizontal polycrystalline alumina plate ( $\text{Al}_2\text{O}_3^{\text{PC}}$ ) (Fig. 1). One surface, over which the drop was later moved, was polished to 160 nm roughness. Before tests, the support was ultrasonically cleaned in the same way as the metal specimens and heated in air at 1273 K for 1 h. After a 15 min hold on the support, each couple was cooled at  $10 \text{ K min}^{-1}$ . The couples were imaged (60 frames  $\text{min}^{-1}$  during heating and 600 frames  $\text{min}^{-1}$  during drop pushing) using a digital camera (Microtron MC1310) with CCD matrix of 1.2 megapixel resolution and equipped with a mirror filter. The collected images were used for automatic calculation of contact angles by ASTRA-View© software [26].

After wettability testing the substrate was examined by scanning electron microscopy (SEM) coupled with energy-dispersive X-ray spectroscopy (EDS) analysis followed by scanning probe microscopy (SPM) characterization. The SPM images scanned in air were obtained using a NTEGRA-THERMA (NT-MDT Co.) apparatus operated in semi-contact mode with the oscil-

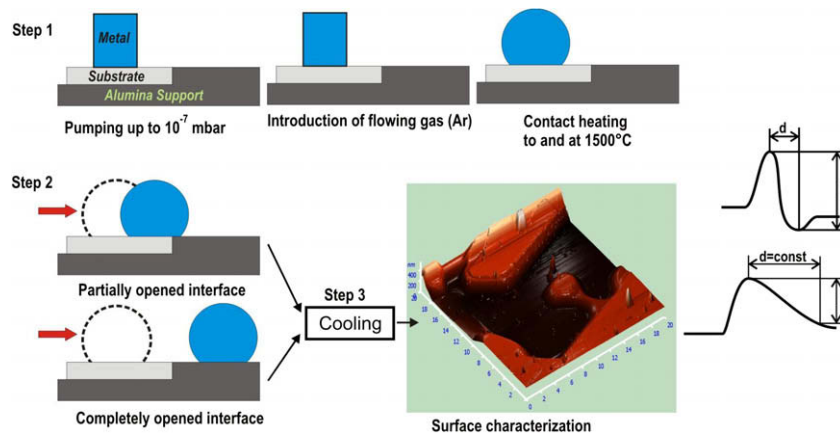


**Figure 1.** Wettability test procedure: (1) heating of the metal/substrate couple to and at the test temperature; (2) in situ opening of the interface by partial or complete droplet replacement; (3) cooling; and (4) characterization of the uncovered area under the drop by scanning probe microscopy. Inset shows ridge size parameters given in Table 1 for: (a) Ni/MgO and NiW10/ $\text{Al}_2\text{O}_3$  and (b) NiW10/MgO.

lating tip (N-type, single crystal Si of  $\sim 15 \mu\text{m}$  height and 6 nm radius of curvature) contacting (“touching”) the surface periodically at the extreme points of its trajectory. Of all known scanning probe microscopes, the one used in this study is characterized by the lowest levels of thermal drift ( $< 10 \text{ nm K}^{-1}$ ) that cause uncontrolled shifting of the probe relative to the sample when temperature gradients exist. The drift of about  $20\text{--}50 \text{ nm h}^{-1}$ , common in commercial scanning probe microscopes, is not critical for large-field characterization, but when the scan size total is in tens of nanometers, the thermal drift becomes a crucial factor since the corresponding range of uncontrolled shift of  $\sim 50\text{--}300 \text{ nm K}^{-1}$  might affect the quality of the SPM images. For each examined sample the length ( $d^r$ ) and height ( $h^r$ ) of the ridge formed due to high-temperature interaction between the droplet and the substrate were measured from the collected SPM data according to the scheme of Figure 1 (inset).

### 3. Results and discussion

Figure 2 illustrates the variation of contact angle with time: Figure 2a shows the data for the period of contact heating from melting to the test temperate (1773 K), and Figure 2b–f shows the data at 1773 K, starting from the first value measured at 1773 K. The test results are summarized in Table 1 together with substrate surface roughness measurements.

Neither pure Ni nor NiW10 alloy wet the MgO(1 0 0) substrate ( $\theta > 90^\circ$ ), and the average contact angles are  $112^\circ$  and  $118^\circ$ , respectively. For Ni/MgO(1 0 0), the final angles in the first and second positions of the drop are identical. The SEM and EDS examinations of tested substrates did not reveal any important differences in their interaction with Ni and NiW10 (some weak surface changes had occurred, distinguished only by dissimilarity in contrast between different regions). Ni was sporadically detected on the surface after testing with Ni drops.

In contrast to the SEM, the SPM images (Fig. 3a–d) show cavities (pits) on MgO(1 0 0) that are reminiscent of dislocation etch pits similar to those reported in Ref. [14]. The three pits over the scanned substrate area in Figure 3b and d are  $\sim 0.75 \times 10^{10} \text{ m}^{-2}$ , a value remarkably close to the dislocation density for single-crystal ceramics (e.g. for sapphire, the value is  $1\text{--}2 \times 10^9 \text{ m}^{-2}$  [28]). Furthermore, etch pits in ceramics are usually triangular, hexagonal or quadrilateral in shape and typically  $\sim 10\text{--}15 \mu\text{m}$  [28] wide, i.e. very similar to those for the pits in Figure 3b and d. Thus, diamond-shaped cavities on MgO in Figure 3b and d could actually be dislocation etch pits that had formed via “thermal etching” under Ni or NiW10 vapor at high temperatures under dynamic vacuum. Similar dislocation etch pits under displaced drops contain mini-droplets (shown below in Fig. 5c and d). The size and number of pits decrease with increasing distance from the drop, suggesting that pit formation is affected by liquid metal vapor (Table 2). For pure Ni, the largest pits in the

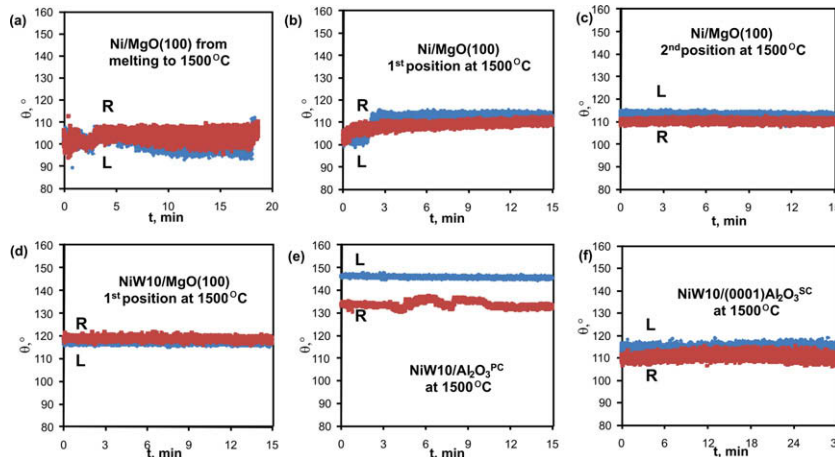


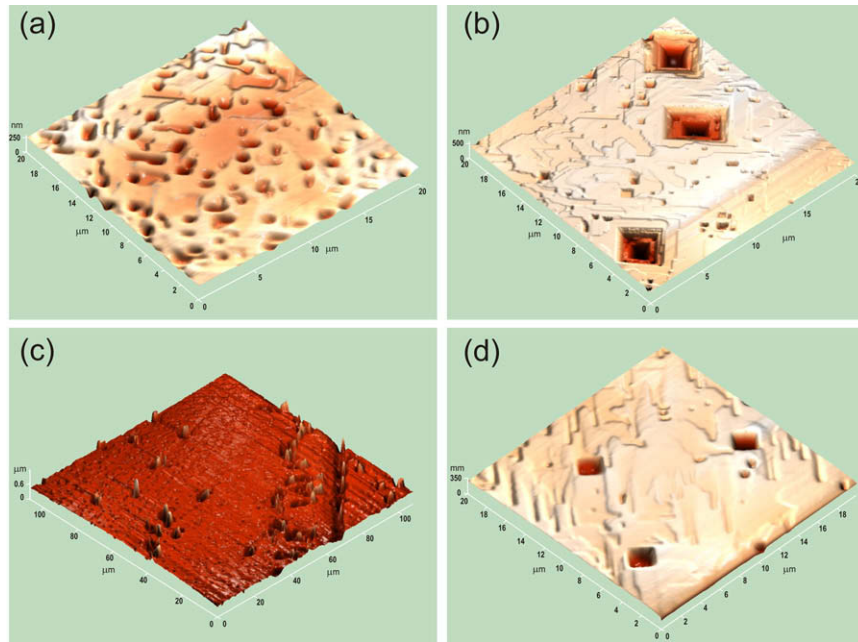
Figure 2. Wettability kinetics in Ni/MgO<sup>SC</sup> (a–c), NiW10/MgO<sup>SC</sup> (d), NiW10/Al<sub>2</sub>O<sub>3</sub><sup>PC</sup> (e) and NiW10/Al<sub>2</sub>O<sub>3</sub><sup>SC</sup> [25] (f) couples (L, left angle; R, right angle).

Table 1. Contact angle ( $\theta$ ) and work of adhesion\* ( $W_a$ ) in examined systems (1773 K, 15 min).

System	Ra [nm]		Ridge size [nm]				$\theta$ [°]			$W_a$ [mN/m]
	Before test	After test**	$h_{av}^r$	$l_{av}^r$	$h_{max}^r$	$l_{max}^r$	Left	Right	Average	
Ni/MgO <sup>SC</sup>	1	22	700	1000	1073	3220	112	111	111.5	1142
	1	9	450	4000	460	4000	117	119	118	950
NiW10/MgO <sup>SC</sup>	160	498					146	132	139	439
NiW10/Al <sub>2</sub> O <sub>3</sub> <sup>SC</sup> [25]	1	5	2100	30,000	3230	59,800	114	110	112	1120

\* Work of adhesion  $W_a = \sigma_{lv}(1 + \cos \theta)$  was calculated using values of  $\sigma_{lv}(\text{Ni}) = 1802.3 \text{ mN/m}$  and  $\sigma_{lv}(\text{NiW10}) = 1790.6 \text{ mN/m}$  from [27].

\*\* Total time of contact was 30 min (including additional 15 min for 2nd drop or on alumina support).



**Figure 3.** SPM images of the MgO(1 0 0) surface (area  $20\ \mu\text{m} \times 20\ \mu\text{m}$ ) after tests showing facets and cavities: (a) far from Ni drop; (b) near Ni drop; (c) under Ni solid sample; (d) near NiW10 drop (1773 K, 15 min followed by interface opening and additional 15 min hold).

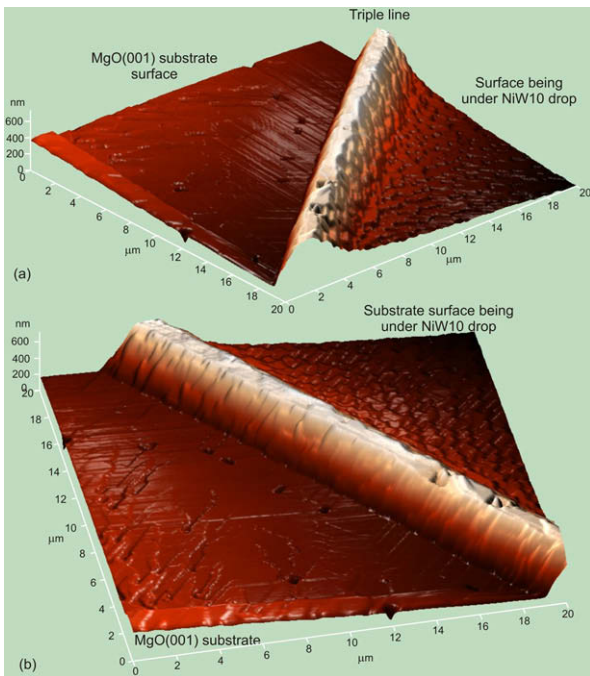


**Figure 4.** SPM 3-D images of the MgO(1 0 0) surface near NiW10 drop showing the structure of ridge surface from (a) the drop-side and (b) outside the drop.

vicinity of drops are about twice as long and three times as deep as those located far from the drop, while the average surface roughness ( $R_a$ , Table 1) becomes more than 20 times higher compared to the virgin substrate. Introduction of 10 wt.% W in Ni reduces the size and number of pits, resulting in nearly 2.5 times smaller increase in  $R_a$  relative to the MgO(1 0 0) surface exposed to pure Ni. Thus, it might be concluded that modifica-

tion of a pristine ceramic surface by metal vapor ahead of an advancing TL takes place even when metal vapor neither reacts with nor condenses at the TL. These observations are important in view of possible crucible degradation above the level of molten metal affecting the lifetime of foundry appliances and the formation of nonmetallic inclusions, particularly in metal pouring by crucible tilting.

SPM also reveals a difference in surface topography under and outside the drop with a prominent ridge dividing these two regions (Fig. 4a and b). Only occasionally are surface cavities distinguished on the drop-covered substrate which was subsequently opened in situ via drop displacement. The opened surface has numerous nanometer-size steps from transformation of the substrate upon contact with liquid metal. In a manner similar to a ridge at the TL, these steps are particularly well distinguished for NiW10 and present facets that probably formed via a mechanism similar to chemical etching because of some dissolution of the oxide in the liquid metal. Due to the high anisotropy of the surface energy of MgO, its dissolution is expected to proceed step by step, thus resulting in a significant change in the substrate surface structure. In particular, it is well distinguished on the ridged surface of NiW10/MgO<sup>SC</sup>, i.e. the drop-side of the ridge has prominent surface facets (Fig. 4a), while its drop-free side is relatively smooth (Fig. 4b). Additionally, different SPM images were obtained for the substrate surface that was in contact with initially solid metal sample (Fig. 3) and for that formed outside of this region after interaction with liquid drops (Figs. 4 and 5). They are in agreement with visual observations under different lightening showing dissimilar brightness of these regions and offer experimental evidence for the effect of primary oxide film on interface formation.

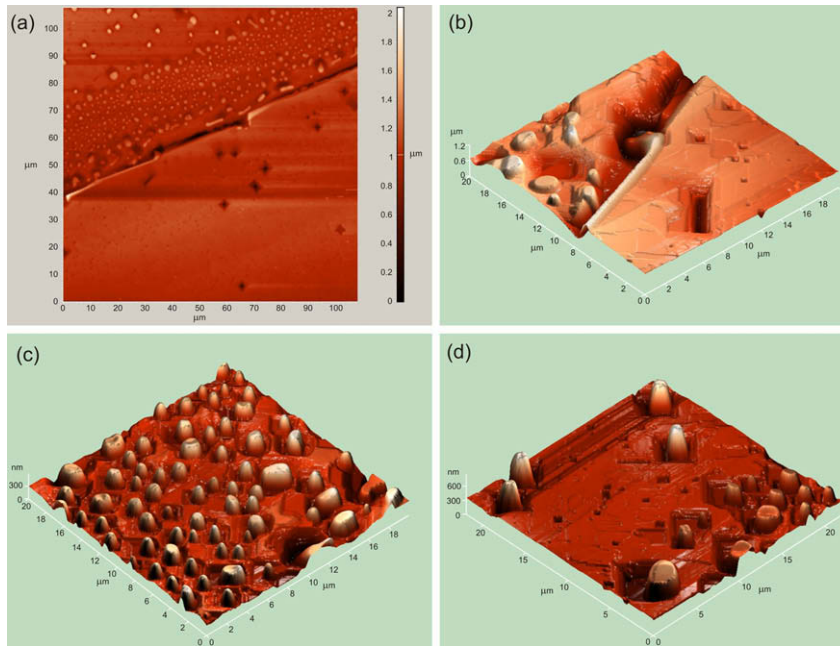


**Figure 5.** SPM images of the MgO(1 0 0) surface formed with Ni: (a) 2-D view and (b) 3-D view showing triple line region; (c and d) 3-D views of surface under a Ni drop.

**Table 2.** Length and depth of surface pits measured by SPM (in [nm]).

Drop	$d_{\max}$	$d_{\text{av}}$	$h_{\max}$	$d_{\max}$	$d_{\text{av}}$	$h_{\max}$	$d_{\max}$	$d_{\text{av}}$	$h_{\max}$
	Far from the droplet			In the drop vicinity			Under drop		
Ni	2000	800	200	5100	4500	700	5500	2200	320
NiW10	1200	600	80	2300	2100	250	3100	600	150

For Ni/MgO<sup>SC</sup>, the ridge is inhomogeneous (Fig. 5a and b), which presumably is related to drop movement due to surface roughening upon heating. A perturbation of ridge continuity at the cross-section with a large pit is shown in Figure 5b. The characteristic feature of surface topography under pure Ni is the presence of numerous small “daughter” droplets inside freshly formed surface cavities (Fig. 5c and d); these droplets formed by rupture of a thin film of the “mother” drop during the latter’s forced displacement. Under a NiW10 drop, such cavities had smooth edges (Fig. 6a and b), while under a Ni drop (Fig. 5c and d), the edges were very sharp, similar to the edges of pits at the drop-free substrate surface. This suggests cavity formation after early displacement of the mother drop and the effect on cavity formation of surrounding small daughter droplets. The small droplets inside pits form due to pushing of the mother drop (Fig. 5c), and the process is akin to spreading butter on a slice of bread. This can also explain how small droplets form inside pits within ridges that develop with NiW10 alloy (Figs. 4a and b and 6a). Another important feature of the substrate under NiW10 drops (Fig. 6c) is the formation of a ridge around a small gas bubble (Fig. 6d and e); such bubbles could be identified even by the naked eye in many NiW10/oxide couples.

The NiW10/MgO<sup>SC</sup> couple displayed an interesting spreading behavior. After a 15 min hold in the first posi-

tion, the NiW10 drop was pushed and partially deposited onto the alumina support in such a way that only  $\sim 2/3$  of the drop’s bottom surface was “seated” on the support. Despite the fact that only  $\sim 1/3$  of the drop base was on the MgO(1 0 0), the drop returned almost to the same position on the MgO(1 0 0) substrate, immediately after taking up the alumina pusher. In the second attempt, the drop was pushed again, positioned wholly on the support and kept for 15 min. Since the support surface had much higher roughness, the difference between the left and the right angles on Al<sub>2</sub>O<sub>3</sub><sup>PC</sup> is noticeable ( $\sim 15^\circ$ ) while the average contact angle value is  $27^\circ$  higher compared to Al<sub>2</sub>O<sub>3</sub><sup>SC</sup> (Table 1). These observations are consistent with the calculations of work of adhesion, which for NiW10/MgO<sup>SC</sup> is more than twice that for NiW10/Al<sub>2</sub>O<sub>3</sub><sup>PC</sup>. This also suggests the reason for the MgO-rich inclusions in Ni-base castings since, during processing, small MgO particles could be detached from the surface of foundry appliances made from polycrystalline MgO-rich ceramics which come into contact with the liquid alloy. Nonwetting behavior in the Ni/MgO system coupled with the significant density difference of MgO and Ni cause enhanced floatation of the MgO particles and their collection to the top of the melt; this makes it reasonable to use bottom metal pouring rather than crucible tilting. During solidification, the MgO inclusions introduced into the melt could

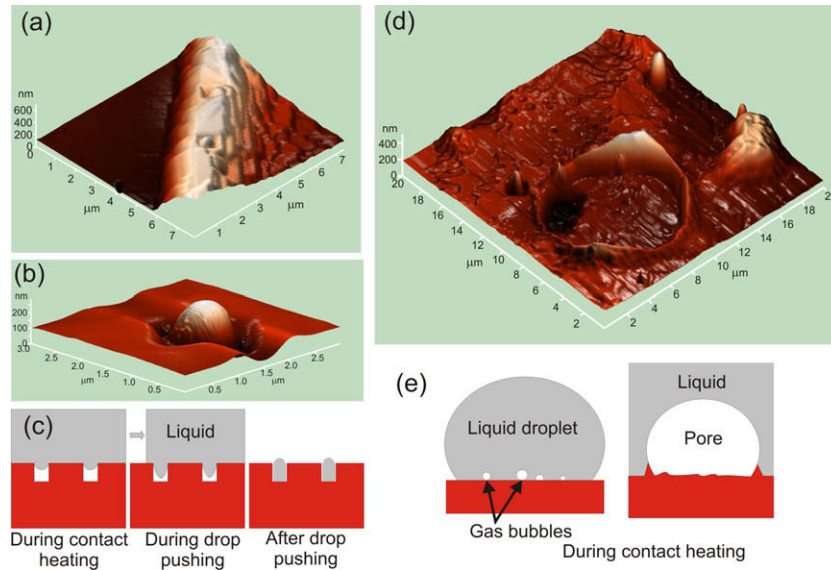


**Figure 6.** (a–c) Selected SPM images of NiW10/MgO(1 0 0) sample showing the ridge (a) and substrate surface (b) under the NiW10 drop and corresponding mechanism of small droplet formation inside surface cavities of MgO(1 0 0) during drop displacement by sideways pushing (c); (d and e) SPM 3-D image of MgO(1 0 0) surface under NiW10 drop (d) and corresponding mechanism of ridging at the local gas bubble/drop/substrate triple line.

be pushed by the solidifying alloy, and hence a directional solidification process accompanied by removal of inclusions is preferable.

#### 4. Summary

On MgO(1 0 0), pure Ni and NiW10 alloy formed contact angles of  $112^\circ$  and  $118^\circ$ , respectively. A special procedure used for in situ opening of the Ni/MgO<sup>SC</sup> and NiW10/MgO<sup>SC</sup> interfaces directly during the sessile drop wettability test at 1773 K and coupled with SPM characterization of interfaces revealed evidence of strong single-crystal substrate surface modification during wettability tests. This was found to be affected by metal evaporation, chemistry of the liquid metal and primary oxide film. The results obtained are consistent with observations in foundry practice showing much better quality of Ni-base castings produced using bottom metal pouring and directional solidification processes.

#### Appendix A. Supplementary data

Supplementary data associated with this article can be found, in the online version, at [doi:10.1016/j.scriptamat.2010.03.003](https://doi.org/10.1016/j.scriptamat.2010.03.003).

#### References

- [1] W.W. Mullins, *Interface Sci.* 9 (2001) 9.
- [2] A.P. Tomsia, E. Saiz, S. Foppiano, R.M. Cannon, in: N. Eustathopoulos, N. Sobczak (Eds.), *High-Temperature Capillarity*, Foundry Research Institute, Cracow, Poland, 1997, pp. 59–81.
- [3] E. Saiz, A.P. Tomsia, R.M. Cannon, *Scripta Mater.* 44 (2001) 159.
- [4] G. Levi, D.R. Clarke, W.D. Kaplan, *Interface Sci.* 12 (2004) 73.
- [5] E. Saiz, R.M. Cannon, A.P. Tomsia, *Adv. Mater.* 12 (24) (2000) 1952.
- [6] J.A. Warren, W.J. Boettinger, A.R. Roosen, *Acta Mater.* 46 (9) (1998) 3247.
- [7] E. Saiz, A.P. Tomsia, *Curr. Opin. Solid State Mater. Sci.* 9 (2005) 167.
- [8] N. Eustathopoulos, *Curr. Opin. Solid State Mater. Sci.* 9 (2005) 152–160.
- [9] O. Dezellus, F. Hodaj, N. Eustathopoulos, *J. Eur. Ceram. Soc.* 23 (2003) 2797.
- [10] N. Sobczak, M. Singh, R. Asthana, *Curr. Opin. Solid State Mater. Sci.* 9 (2005) 241.
- [11] V.E. Henrich, *Surf. Sci.* 57 (1997) 385.
- [12] J.R. Heffelfinger, C.B. Carter, *Surf. Sci.* 389 (1987) 188.
- [13] R. Plass, J. Feller, M. Gajdardziska-Josifovska, *Surf. Sci.* 414 (1998) 26.
- [14] D.R. Giese, F.J. Lamelas, H.A. Owen, R. Plass, M. Gajdardziska-Josifovska, *Surf. Sci.* 457 (2000) 326.
- [15] K. Sangwal, F. Sanz, P. Gorostiza, *Surf. Sci.* 424 (1999) 139.
- [16] C. Iwamoto, S.-I. Tanaka, *Acta Mater.* 50 (2002) 749.
- [17] N. Eustathopoulos, N. Sobczak, A. Passerone, K. Nogi, *J. Mater. Sci.* 40 (9–10) (2005) 2271.
- [18] S.S. Perry, P.B. Merrill, *Surf. Sci.* 383 (1997) 268.
- [19] O. Robach, G. Renaud, A. Barbier, *Surf. Sci.* 401 (1998) 227.
- [20] K. Fukui, Y. Iwasawa, *Surf. Sci.* 441 (1999) 529.
- [21] T.V. Ashworth, C.L. Pang, P.L. Wincott, D.J. Vaughan, G. Thornton, *Appl. Surf. Sci.* 210 (2003) 2.
- [22] P. Sheng, H. Fujii, T. Matsumoto, K. Nogi, *Scripta Mater.* 48 (2003) 779.
- [23] N. Sobczak, R. Nowak, W. Radziwill, J. Budzioch, A. Glenz, *Mater. Sci. Eng.* 495A (2008) 43.
- [24] Y. Hao, G. Meng, Y. Zhou, M. Kong, Q. Wei, M. Ye, L. Zhang, *Nanotechnology* 17 (2006) 5006.
- [25] N. Sobczak, R. Asthana, R. Nowak, B. Korpala, G. Burda, *Trans. FRI*, 2010, in press.
- [26] *ASTRA Reference Book*, IENI Report, 2007.
- [27] F. Xiao, L. Liu, R. Yang, H. Zhao, L. Fang, C. Zhang, *Trans. Non-Ferrous Met. Soc. China* 18 (2008) 1184.
- [28] J. Xiao, S. Yin, M. Shao, X. Zhang, *J. Crystal Growth* 266 (2004) 519.